The work by Cai et al. investigates the SOA formation in downwind regions of urban areas, focusing on the PRD region of China in the fall of 2019. The FIGAERO-CIMS was employed to analyze the molecular composition and volatility of organic compounds in both gas and particle phases. The findings highlight significant daytime SOA formation driven by gas-particle partitioning, influenced by urban pollutants such as NOx and volatile organic compounds (VOCs). The paper is well-structured, clearly written, and a valuable contribution to the field of atmospheric sciences, particularly in understanding the dynamics of SOA formation in urban-influenced suburban areas. With the following comments addressed, it would be suitable for publication in ACP.

1. The aBBOA factor appears to have a lower O:C and a higher H:C compared to the BBOA factor (Figure S3). This is contrary to what it is expected for aging. This makes me wonder how these PMF factors were exactly assigned. Some explanation will be helpful.

Reply: We appreciate the reviewer for this valuable suggestion. The lower O:C ratio and higher H:C ratio implies that aBBOA was likely formed through oxidation of biomass burning precursors rather the aging process of BBOA. To avoid any confusion, we rename this factor as biomass burning SOA (BBSOA). We have modified section 2.2.2 by providing more description of these factors.

"The PM_1 chemical composition was measured by a soot particle aerosol mass spectrometer (SP-AMS, Aerodyne Research, Inc., USA). The details of the operation and data analysis can be found in Kuang et al. (2021). Source apportionment was performed for organic aerosols in the bulk PM_1 using positive matrix factorization (PMF). The organic aerosol could be divided into six components, including two primary OA factors and four secondary OA factors. The mass spectral profiles of six OA factors are shown in Figure S3. The timeseries and diurnal variation of these factors are presented in Figure S4.

The primary OA factors include hydrocarbon-like OA (HOA), mainly contributed by traffic and cooking emissions and biomass burning OA (BBOA) originating from biomass burning combustion. The HOA was identified by hydrocarbon ions $C_xH_y^+$. Owing to the prominent hydrocarbon ions and low O:C value (0.10), HOA could be attributed to primary emission from cooking and traffic. The BBOA was recognized by the markers $C_2H_4O_2^+$ (m/z 60.022, 0.5%) and $C_3H_5O_2^+$ (m/z 73.029, 0.4%), which are considered tracers for biomass burning OA (Ng et al., 2011).

The SOA factors include biomass burning SOA (BBSOA) likely formed from oxidation of biomass burning emission, less oxygenated OA (LOOA) provided by strong daytime photochemical formation, more oxygenated OA (MOOA) related to regional transport, and nighttime-formed OA (Night-OA) contributed by secondary formation during nighttime. The BBSOA was likely formed through oxidation of biomass burning precursors, which was supported by the evening peak at about 19:00 LT (Fig. S4). BBSOA showed a similar variation trend with $C_6H_2NO_4^+$, which might be contributed by oxidation of gaseous precursors from biomass burning emissions (Wang et al., 2019; Bertrand et al., 2018). The significant afternoon peak of LOOA indicates its formation through photochemical reactions, which would be detailly discussed in section 3.1. The negligible diurnal variation and the highest O:C value (1.0) of MOOA suggested that it could be aged OA resulting from long-range transport. Night-OA was formed through NO_3 nighttime chemistry, supported by

a pronounced evening elevation and positive correlation with nitrate (R=0.67).The detailed determination of PMF factors has been found in Kuang et al. (2021) and Luo et al. (2022).

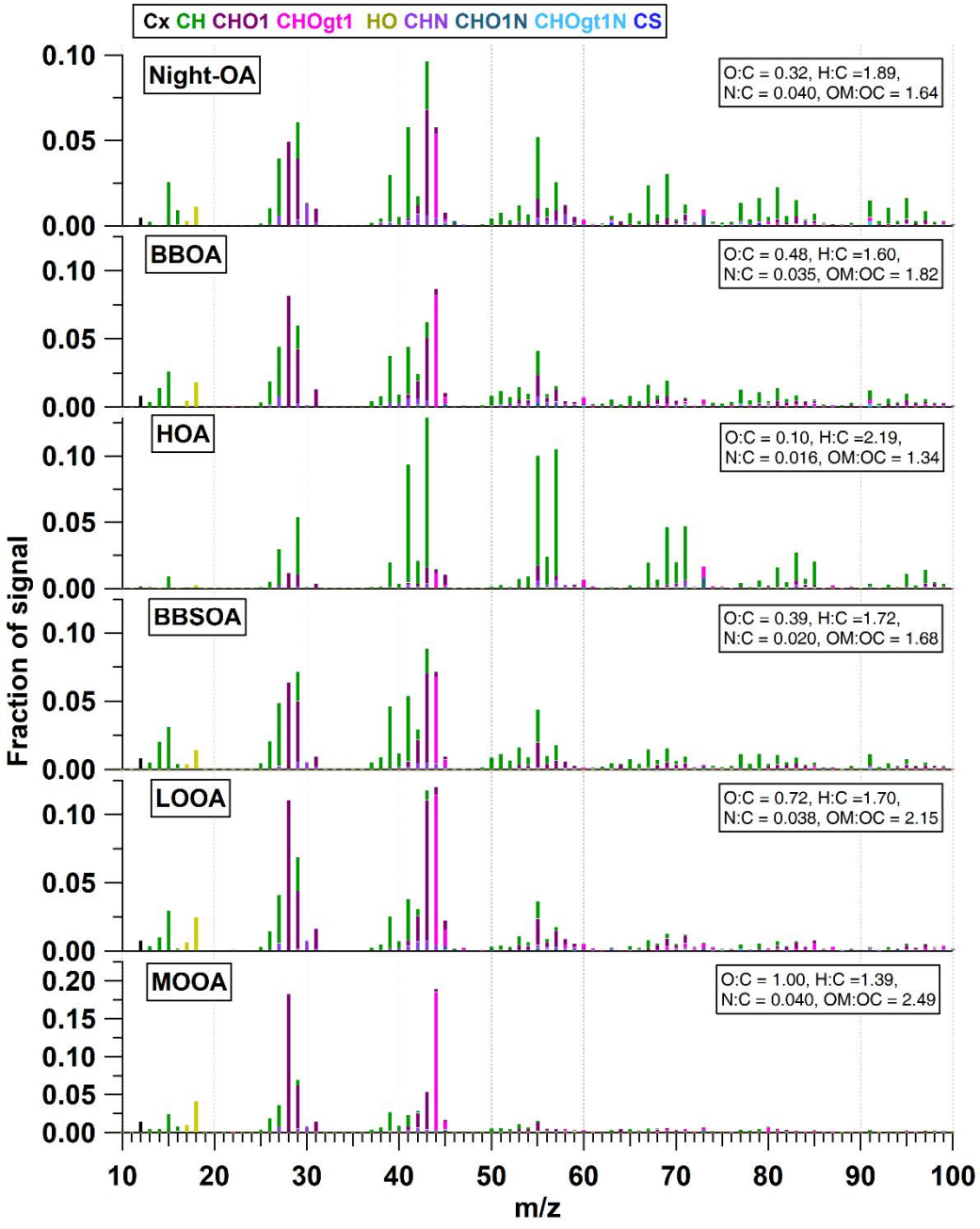

Figure S3. Mass spectral profile of six OA factors. The colors represent different family groups.

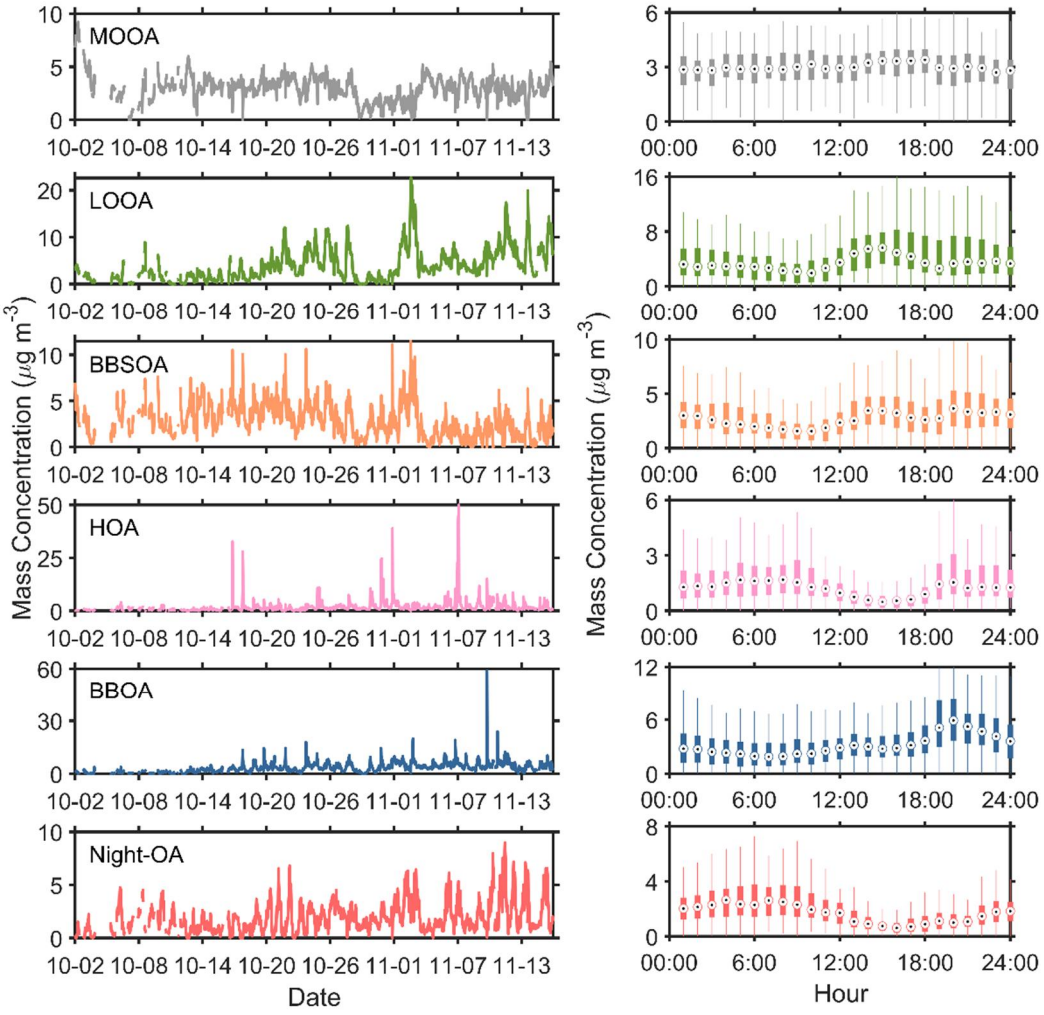

Figure S4. Timeseries and diurnal variation of six OA factors.

”

2. Line 179-183: There does not seem to be a clear trend between mass loading and Tmax and the calibration mass loading range does not cover the campaign mass loading center (Figure S5). Can the authors explain the rationale of picking the fitting parameters of the experiment with Dp 200 nm and mass loading = 407 ng rather than for example the parameters from fitting all experiments? What is the direction of bias introduced by this choice?

Reply: We appreciate the reviewer for this valuable suggestion. Wang and Hildebrandt Ruiz (2018) indicated that the relationship between mass loading and T_{max} can be described by a sigmoid function. The non-monotonic trend between mass loading and T_{max} could partly owing to the fact that the mass loading reached the “plateau” region in the sigmoid function. We also performed the

T_{max} calibration based on the syringe deposition method. Our results suggest that the T_{max} value does not always increase with the increase in mass loading (fig. 2.1). Huang et al. (2018) suggested that the non-linear correlation between T_{max} shift and mass loading might be due to matrix or saturation effects. Considering the T_{max} dependence might reach a plateau, the increase in mass loading might play a minor effect in our calibration results. Thus, we did not perform any further experiments with higher mass loading. The mass loading and average particle volume size distribution (PVSD) shows that the mass loading centered at about 602 ng and the PVSD centered at about 400 nm. However, generating particles larger than 250 nm is challenging for our atomizer. Thus, the experiment with a Dp of 200 nm and mass loading of 407 ng were utilized because mass loading and diameter are the closest to the ambient samples.

We added some discussion about this phenomenon and choosing the fitting parameters in line 205-213,

"Note that the T_{max} can vary with mass loading, and it is necessary to consider for estimation the relationship between T_{max} and C^* (Wang and Hildebrandt Ruiz, 2018). Our calibration results demonstrated that the correlation between T_{max} shift and mass loading was not linear, which may be attributed to matrix or saturation effects (Huang et al., 2018). During the measurement, the collected mass loading centered at about 620 ng and the particle volume size distribution (PVSD) centered at about 400 nm (Fig. S6). Thus, the fitting parameters (a=-0.206 and a=3.732) of the calibration experiment with a diameter of 200 nm and mass loading of 407 ng were adopted in the C^* calculation, since the mass loading and diameter are the closest to the ambient samples."

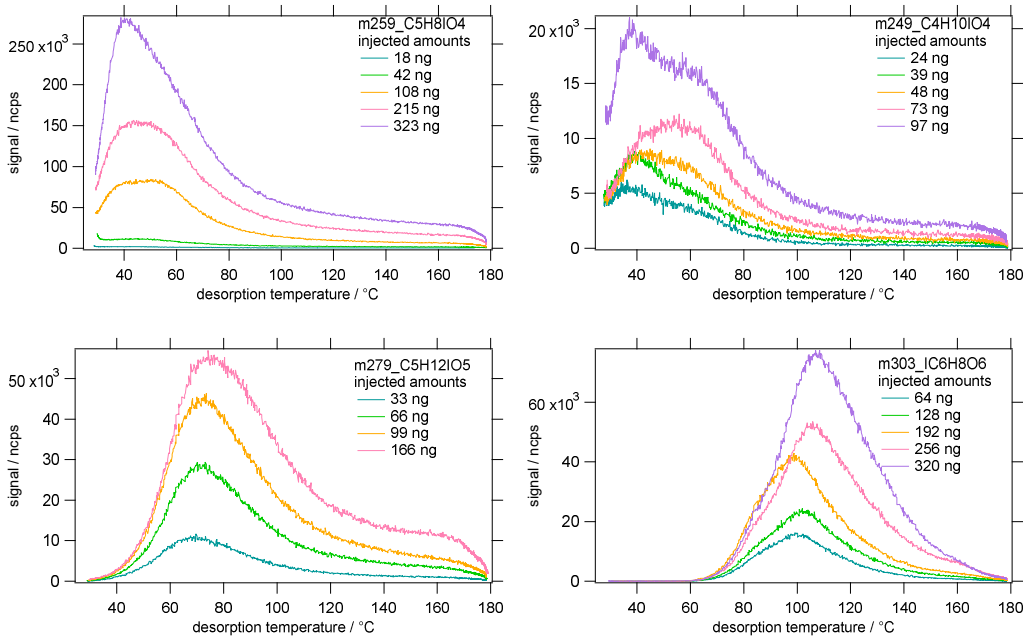

Figure 2.1 Thermograms for different compounds at different loading conditions.

3. Line 184-186: it would be helpful to describe how the black line in Figure S6 that differentiates the oxidation pathways was determined in light of existing literature in a sentence or two.

Reply: We thank the reviewer for this valuable suggestion. We have added some descriptions about how to determine the pathway in the main text. Also, we have revised the slope of black line in the Van-Krevelen diagram, since the previous one was a copy mistake.

Line 214-218, "For gas-phase organic compounds (organic vapors), we first divided them into two groups based on their potential oxidation pathways (multi-generation OH oxidation and autoxidation, solid line in Fig. S7) and then used different parameters in their volatility estimation. The classification of pathways was based on the molecular characteristics of oxidation products of aromatics and monoterpene, respectively (Wang et al., 2020).

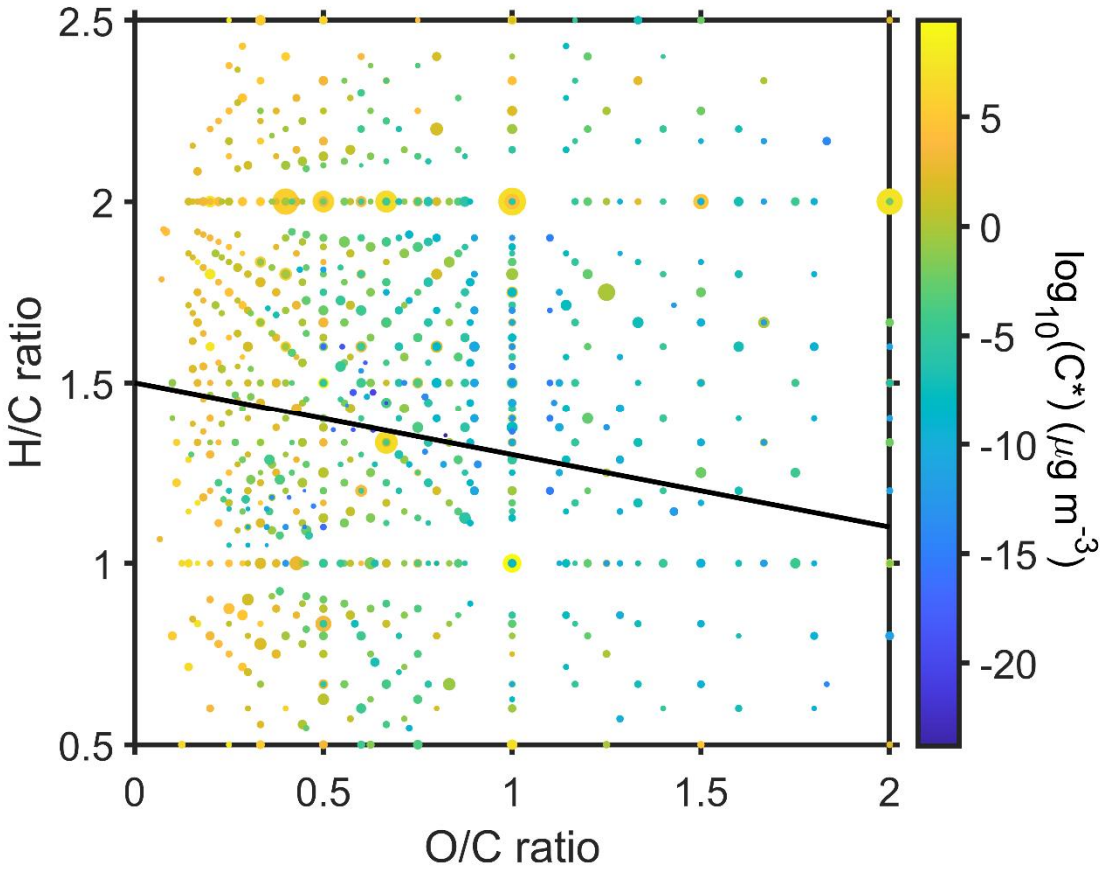

Figure S7. Van-Krevelen diagram (O/C ratio versus H/C ratio) of gas-phase organic compounds measured by FIGAERO-CIMS. The symbol size is proportional to the mass concentration of organic vapors and the color code represents the volatility. The black solid line divided the organic vapors potentially formed through the autoxidation pathway (upper regime) and multi-generation OH oxidation pathway (lower regime), based on the oxidation products aromatics and monoterpene, respectively (Wang et al., 2022; Wang et al., 2020). "

Line 225-227, "It should be noted that this method can only roughly distinguish the formation pathways of ambient organic vapors, since it is based on the oxidation products of specific species in a laboratory study."

4. Line 217-220: These observation data used to constrain F0AM simulations were not mentioned in the instrumentation section of the paper. Are these collocated and published data? Adding a brief description would provide necessary context.

Reply: We thank the reviewer for this valuable comment. These observation data were measured by a series of instruments during the campaign. The background concentration of CH_4 was set as 1.8 ppm (Wang et al., 2011). We added a brief description of the corresponding instruments in the instrumentation section.

Line 172-180,

"**2.2.4 Other parameters**

The non-methane hydrocarbons (NMHC) were measured by an online GC-MS-FID (Wuhan Tianhong Co., Ltd, China). The concentration of oxygenated VOCs, including formaldehyde (HCHO) and acetaldehyde (CH_3CHO), were measured using high-resolution proton transfer reaction time-of-flight mass spectrometry (PTR-ToF-MS, Ionicon Analytik, Austria). HONO was detected by the gas and aerosol collector (GAC) instrument (Dong et al., 2012). Trace gases, including O_3, NO_x, and CO, were measured by gas analyzers (model 49i, 42i, and 48i, Thermo Scientific, US). Meteorological parameters (i.e., wind speed, wind direction, and temperature) were measured by a weather station (Vantage Pro 2, Davis Instruments Co., US). "

We also modified the sentence in Line 265-268,

"The simulation was constrained with the observation data of non-methane hydrocarbons (NMHC), HCHO, CH_3CHO, NO, CO, HONO, and meteorological parameters (RH, temperature, photolysis rates, and pressure). The background concentration of CH_4 was set as 1.8 ppm (Wang et al., 2011)."

5. Line 302: The term "non-condensable" ($C*$ >10^0.5 μg m^{-3}) is a bit confusing. These vapors are apparently condensable SVOCs that would partition between gas and particle phases. Is this definition based on specific literature? Clarifying this term would enhance understanding.

Reply: We appreciate the reviewer for this valuable suggestion. Our assignment of organic vapors was based on Wang et al. (2022). Wang et al. (2022) integrated organic vapor from the lowest volatility bin to $C^* \leq 10^{0.5}$ μg m^{-3} and regard them as condensable vapors. The mass flux of condensable vapors between gas and particle phase was calculated. Nie et al. (2022) calculated the contribution of condensing organic vapor to the formation of SOA. For organic vapor with relatively lower volatility ($C^* \leq 0.01$ μg m^{-3}), the condensation to particle-phase was regarded as irreversible. We noticed that using the name "non-condensable organic vapors" and "condensable organic vapors" could lead to confusion, since "non-condensable organic vapors" can also reach the particle phase through gas-particle partitioning. Thus, we modified the classification, ELVOC and LVOC are classified as low volatility organic vapors ($C^* \leq 0.3$ μg m^{-3}), while SVOC, IVOC and VOC fall into

another category regarded as high volatility organic vapors ($C^* > 0.3$ μg m^{-3}). The corresponding sentences have been revised.

6. Line 308-313: I wonder if the authors can quantitatively estimate the contribution of the "non-condensable" organic vapors to the total organic aerosol mass to strengthen this point. The saturation vapor concentration for the gas-phase organic vapors have already been estimated. The organic aerosol mass loadings from SP-AMS are available. Then the particle-phase concentrations of these compounds can be calculated based on equilibrium partitioning and compared with the mass that FIGAERO is missing out (mass balance).

Reply: We appreciate the viewer for this valuable suggestion. We have estimated the contribution of high volatility organic vapors (SVOC+IVOC+VOC) to the OA concentration ($Estimated\ OA_{HVgas}$) based on the following equation:

$$Estimated\ OA_{HVgas} = \sum_i C_{i,g} f_i \quad (1)$$

where $C_{i,g}$ is the gas-phase concentration of species i. f_i is the fraction of species i in the particle phase and is defined as:

$$f_i = \frac{C_{OA}}{C_{OA}+C_i^*(T)} \quad (2)$$

where C_{OA} is the concentration of OA measured by the SP-AMS, and $C_i^*(T)$ is the saturation concentration of species i at temperature (T). The temperature-dependent $C_i^*(T)$ was obtained by (Nie et al., 2022):

$$\log_{10} C_i^*(T) = \log_{10} C_i^*(300K) + \frac{\Delta H_{vap,i}}{Rln(10)}\left(\frac{1}{300} - \frac{1}{T}\right) \quad (3)$$

$$\Delta H_{vap,i} = -5.7\log_{10} C_i^*(300K) + 129 \quad (4)$$

where $\Delta H_{vap,i}$ is the enthalpy of vaporization and can be estimated based on $\log_{10} C_i^*(300K)$.

Our results show that the estimated contribution of high volatility organic vapors was higher (peaked at about 1.17 μg m^{-3}) during the urban air masses period (Fig. 6.1 a). Correspondingly, we observed an enhancement in the measured concentration of these species (peaked at about 10.32 μg m^{-3}) in the particle-phase (Fig. 6.1 b). This implies that the increase in high volatility organic vapors might contribute to the daytime SOA formation. However, the estimated contribution was much lower than the measured value. It suggests that using the equilibrium equation might not be able to fully explain the increase of LOOA contributed by the high volatility organic vapors during the urban air masses period. Nie et al. (2022) indicated that the estimation of OA contribution through the equilibrium equation can be easily disturbed by varied meteorological processes, which would lead to uncertainties in the calculations.

Moreover, the gas-particle equilibrium theory assumes that particles are droplets and that the high volatility species in the particle-phase could reach a reversible equilibrium with the gas-phase concentration. However, some studies indicate that this assumption significantly overestimates the volatility of these species in the particle-phase and underestimate the contribution of high volatility organic vapors to the SOA concentration (Kolesar et al., 2015; Cappa and Wilson, 2011). This is because particles might exist in a glassy state rather than a liquid state. It was consistent with the difference of the volatility distribution of these species between the particle- and gas-phase (Fig. 6.2a). The volatility in the particle-phase was centered at a $log_{10}C^*$ of -1, while that in the gas-phase

showed a higher concentration of $log_{10}C^*$=6-8 μg m^{-3}, implying that the volatility of these compound in the particle-phase could higher than that in the gas-phase.

Another possible explanation is that the corresponding species in the particle-phase could be the decomposition products of low volatility compounds, leading to a higher concentration than expected. We further investigate the difference between the measured and estimated concentration of different high volatility species (Fig. 6.2b). The measured concentration was systematically higher than the estimated value. The higher measured concentration of $C_2H_2O_4I^-$ could be owing to the decomposition of low volatility spices, as the desorption signal peaked at the ELVOC region (Fig. 6.2c). However, for higher molecular weight compounds, the corresponding T_{max} values were in the LVOC region, suggesting that these species might not be the decomposition products. This suggests that the decomposition products might play a minor effect in the difference between the measured and estimated concentration.

Taken together, these results suggest the increase in high volatility organic vapors might lead to the daytime enhancement of SOA during urban air masses period. However, this contribution might be underestimated using gas-particle equilibrium theory, since the volatility of organic aerosol may differ significantly from the volatility determined by the equilibrium theory.

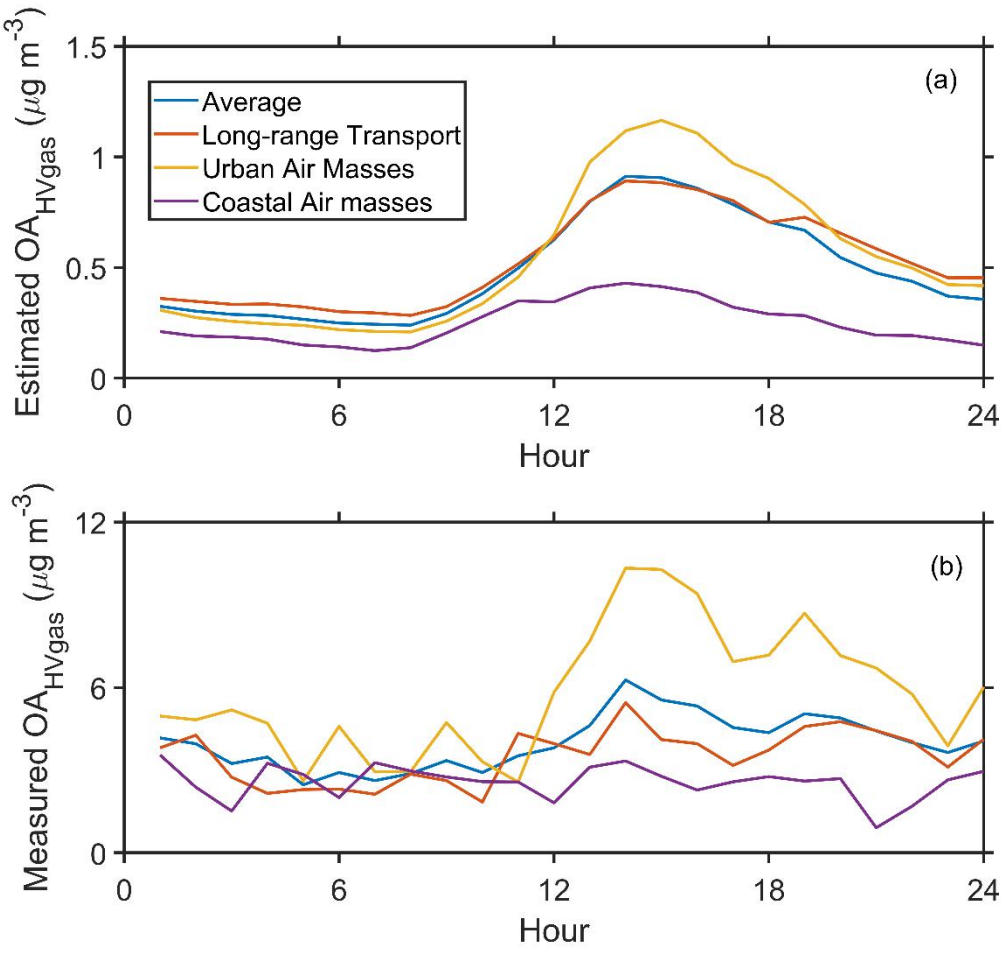

Figure 6.1 The diurnal variation of (a) the estimated contribution of high volatility organic vapors to the OA and (b) the total concentration of corresponding species in the particles-phase measured by the FIGAERO CIMS.

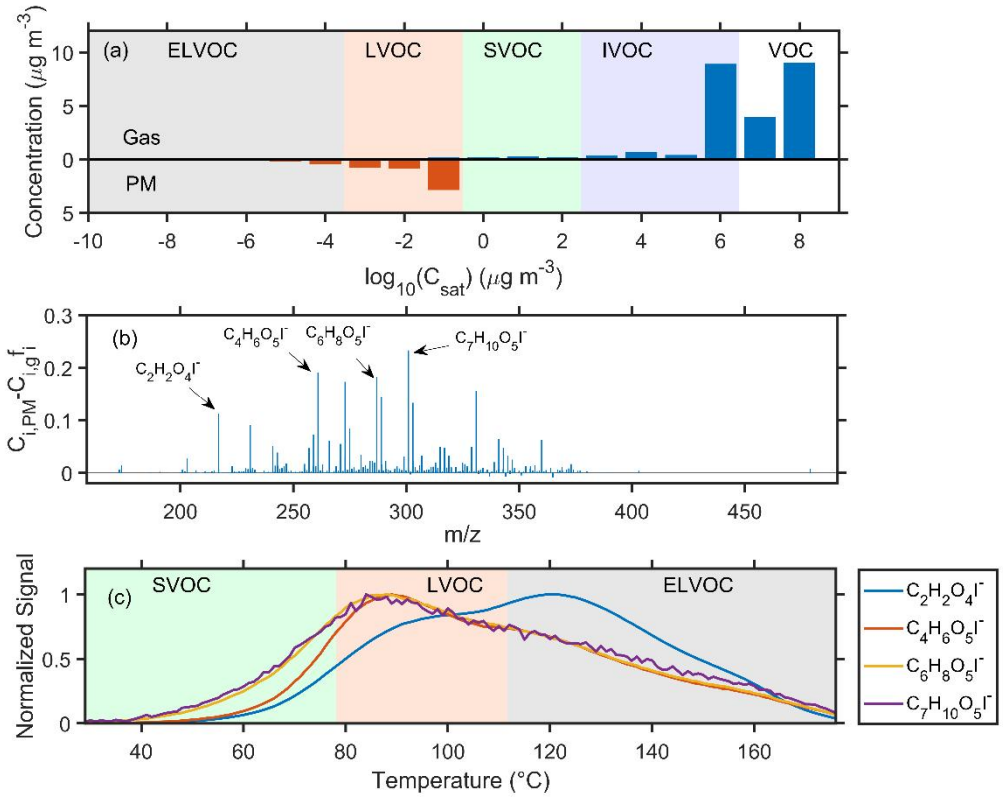

Figure 6.2 (a) The average volatility distribution of high volatility organic vapors in the gas-phase and particle-phase. (b)The average difference between the measured concentration in the particle-phase ($C_{i,PM}$) and the estimated concentration ($C_{i,g}f_i$) of different compounds in the high volatility organic vapors. (c) The average thermograms of $C_2H_2O_4I^-$, $C_4H_6O_5I^-$, $C_6H_8O_5I^-$, and $C_7H_{10}O_5I^-$.

We added a section introducing the estimation of OA contribution based on equilibrium theory in the Methodology section,

"**2.3.4 Estimation of OA contributed by high volatility organic vapors**

Organic vapors with higher volatility (SVOC+IVOC+VOC, C^* >0.3 μg m^{-3}) can easily reach an equilibrium between the gas and particle phase. Thus, the contribution of high volatility organic vapors to OA concentration (OA_{HVgas}) through gas-particle partitioning can be estimated as following:

$$OA_{HVgas} = \sum_i C_{i,g} f_i \quad (7)$$

where $C_{i,g}$ is the gas-phase concentration of species i. f_i is the fraction of species i in the particle phase and is defined as:

$$f_i = \frac{C_{OA}}{C_{OA}+C_i^*(T)} \quad (8)$$

where C_{OA} is the concentration of OA measured by the SP-AMS, and $C_i^*(T)$ is the saturation concentration of species i at temperature (T). The temperature-dependent $C_i^*(T)$ was obtained by

(Nie et al., 2022):

$$\log_{10} C_i^*(T) = \log_{10} C_i^*(300K) + \frac{\Delta H_{vap,i}}{Rln(10)}\left(\frac{1}{300} - \frac{1}{T}\right) \quad (9)$$

$$\Delta H_{vap,i} = -5.7\log_{10} C_i^*(300K) + 129 \quad (10)$$

where $\Delta H_{vap,i}$ is the enthalpy of vaporization and can be estimated based on $\log_{10} C_i^*(300K)$.

"

We also add a section about the contribution of high volatility organic vapors,

"**3.3 The contribution of high volatility organic vapors to SOA formations**

In the previous section, we found that the significant enhancements in LOOA during the urban air masses period might be attributed to the high volatility organic vapors through gas-particle partitioning. The contribution of high volatility organic vapors to the OA concentration via equilibrium partitioning can be estimated based on eq. (7). Our results show that the estimated contribution of high volatility organic vapors (estimated OA_{HVgas}) was higher (peaked at about 1.17 μg m^{-3}) during the urban air masses period (Fig. 6a). Correspondingly, we observed an enhancement in the measured concentration of these species in the particle-phase (measured OA_{HVgas}, peaked at about 10.32 μg m^{-3}, Fig. 6b). This implies that the increase in high volatility organic vapors might significantly contribute to the daytime SOA formation during the urban air masses period. However, the estimated contribution was much lower than the measured value. It suggests that using the equilibrium equation might not be able to fully explain the increase of LOOA contributed by the high volatility organic vapors during the urban air masses period. Nie et al. (2022) indicated that the estimation of OA contribution through the equilibrium equation can be easily disturbed by varied meteorological processes, which would lead to uncertainties in the calculations.

Moreover, the gas-particle equilibrium theory assumes that particles are droplets and that the high volatility species in the particle-phase could reach a reversible equilibrium with the gas-phase concentration. However, some studies indicate that this assumption significantly overestimates the volatility of these species in the particle-phase and underestimate the contribution of high volatility organic vapors to the SOA concentration (Kolesar et al., 2015; Cappa and Wilson, 2011). This is because particles might exist in a glassy state rather than a liquid state. It was consistent with the difference of the volatility distribution of these species between the particle- and gas-phase (Fig. 7a). The volatility in the particle-phase was centered at a $log_{10}C^*$ of -1, while that in the gas-phase showed a higher concentration of $log_{10}C^*$=6-8 μg m^{-3}, implying that the volatility of these compounds in the particle-phase could lower than that in the gas-phase.

Another possible explanation is that the corresponding species in the particle-phase could be the decomposition products of low volatility compounds, leading to a higher concentration than expected. We further investigate the difference between the measured and estimated concentration of different high volatility species (Fig. 7b). The measured concentration was systematically higher than the estimated value. The higher measured concentration of $C_2H_2O_4I^-$ could be owing to the decomposition of low volatility spices, as the desorption signal peaked at the ELVOC region (Fig. 7c). However, for higher molecular weight compounds, the corresponding T_{max} values were in the LVOC region, suggesting that these species might not be the decomposition products. This implies

that the decomposition products might play a minor effect in the difference between the measured and estimated concentration.

Taken together, these results suggest the increase in high volatility organic vapors could promote the daytime enhancement of SOA during urban air masses period. However, this contribution might be underestimated using gas-particle equilibrium theory, since the volatility of organic aerosol may differ significantly from the volatility determined by the equilibrium theory.

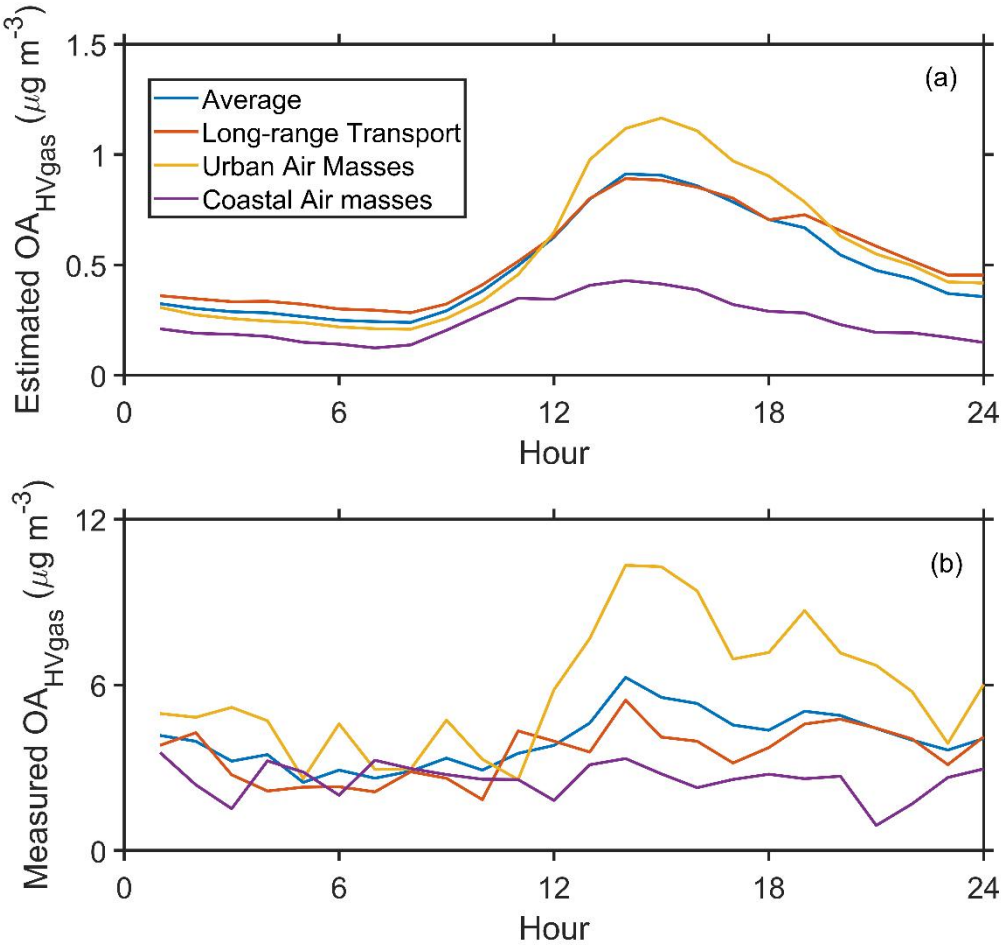

Figure 6. The diurnal variation of (a) the estimated contribution of high volatility organic vapors to the OA (Estimated OA_{HVgas}) and (b) the total concentration of corresponding species in the particles-phase measured by the FIGAERO CIMS.

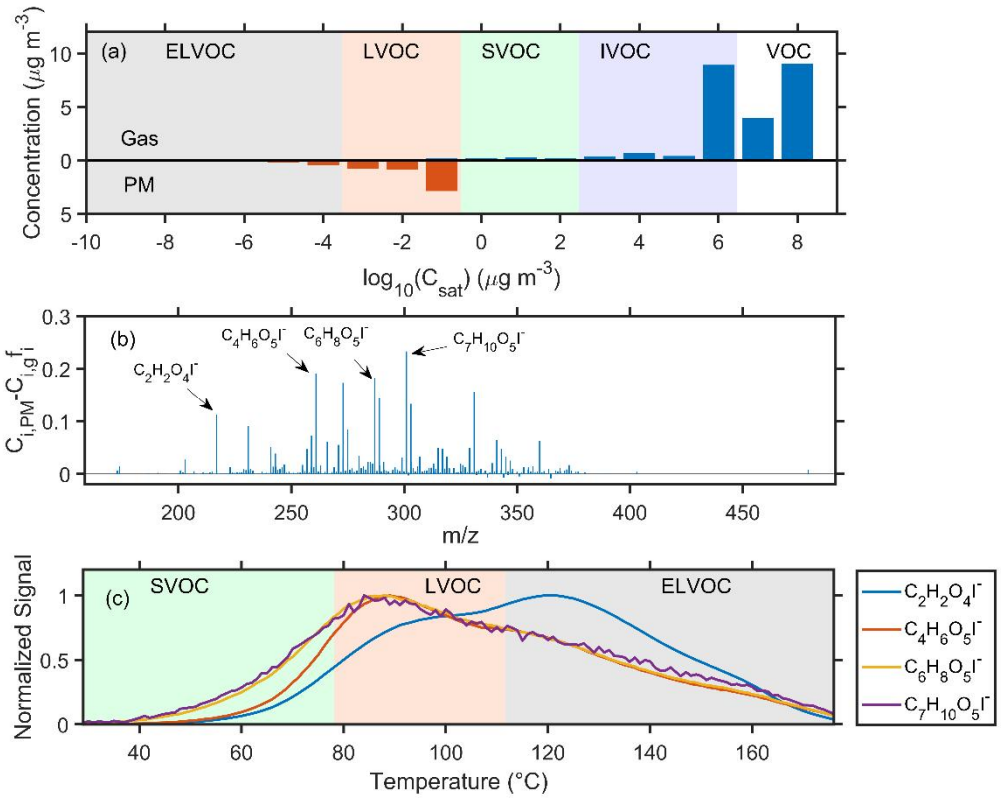

Figure 7. (a) The average volatility distribution of high volatility organic vapors in the gas-phase and particle-phase. (b)The average difference between the measured concentration in the particle-phase ($C_{i,PM}$) and the estimated concentration ($C_{i,g}f_i$) of different compounds in the high volatility organic vapors. (c) The average thermograms of $C_2H_2O_4I^-$, $C_4H_6O_5I^-$, $C_6H_8O_5I^-$, and $C_7H_{10}O_5I^-$.

”

Technical corrections:

Line 180: “estimation” should be “estimating”.

Reply: It has been revised.

Line 390: “ddramatic” should be “dramatic”.

Reply: It has been revised.

SI Line 63: Figure S7 was mislabeled as Figure S8.

Reply: It has been revised.

Reference

Bertrand, A., Stefenelli, G., Jen, C. N., Pieber, S. M., Bruns, E. A., Ni, H., Temime-Roussel, B., Slowik, J. G., Goldstein, A. H., El Haddad, I., Baltensperger, U., Prévôt, A. S. H., Wortham, H., and Marchand, N.: Evolution of the chemical fingerprint of biomass burning organic aerosol during aging, Atmos. Chem. Phys., 18, 7607-7624, 10.5194/acp-18-7607-2018, 2018.

Cappa, C. D. and Wilson, K. R.: Evolution of organic aerosol mass spectra upon heating: implications for OA phase and partitioning behavior, Atmos. Chem. Phys., 11, 1895-1911, 10.5194/acp-11-1895-2011, 2011.

Dong, H. B., Zeng, L. M., Hu, M., Wu, Y. S., Zhang, Y. H., Slanina, J., Zheng, M., Wang, Z. F., and Jansen, R.: Technical Note: The application of an improved gas and aerosol collector for ambient air pollutants in China, Atmos. Chem. Phys., 12, 10519-10533, 10.5194/acp-12-10519-2012, 2012.

Huang, W., Saathoff, H., Pajunoja, A., Shen, X., Naumann, K. H., Wagner, R., Virtanen, A., Leisner, T., and Mohr, C.: α-Pinene secondary organic aerosol at low temperature: chemical composition and implications for particle viscosity, Atmos. Chem. Phys., 18, 2883-2898, 10.5194/acp-18-2883-2018, 2018.

Kolesar, K. R., Li, Z., Wilson, K. R., and Cappa, C. D.: Heating-Induced Evaporation of Nine Different Secondary Organic Aerosol Types, Environmental Science & Technology, 49, 12242-12252, 10.1021/acs.est.5b03038, 2015.

Kuang, Y., Huang, S., Xue, B., Luo, B., Song, Q., Chen, W., Hu, W., Li, W., Zhao, P., Cai, M., Peng, Y., Qi, J., Li, T., Wang, S., Chen, D., Yue, D., Yuan, B., and Shao, M.: Contrasting effects of secondary organic aerosol formations on organic aerosol hygroscopicity, Atmos. Chem. Phys., 21, 10375-10391, 10.5194/acp-21-10375-2021, 2021.

Luo, B., Kuang, Y., Huang, S., Song, Q., Hu, W., Li, W., Peng, Y., Chen, D., Yue, D., Yuan, B., and Shao, M.: Parameterizations of size distribution and refractive index of biomass burning organic aerosol with black carbon content, Atmos. Chem. Phys., 22, 12401-12415, 10.5194/acp-22-12401-2022, 2022.

Ng, N. L., Canagaratna, M. R., Jimenez, J. L., Zhang, Q., Ulbrich, I. M., and Worsnop, D. R.: Real-Time Methods for Estimating Organic Component Mass Concentrations from Aerosol Mass Spectrometer Data, Environmental Science & Technology, 45, 910-916, 10.1021/es102951k, 2011.

Nie, W., Yan, C., Huang, D. D., Wang, Z., Liu, Y., Qiao, X., Guo, Y., Tian, L., Zheng, P., Xu, Z., Li, Y., Xu, Z., Qi, X., Sun, P., Wang, J., Zheng, F., Li, X., Yin, R., Dallenbach, K. R., Bianchi, F., Petäjä, T., Zhang, Y., Wang, M., Schervish, M., Wang, S., Qiao, L., Wang, Q., Zhou, M., Wang, H., Yu, C., Yao, D., Guo, H., Ye, P., Lee, S., Li, Y. J., Liu, Y., Chi, X., Kerminen, V.-M., Ehn, M., Donahue, N. M., Wang, T., Huang, C., Kulmala, M., Worsnop, D., Jiang, J., and Ding, A.: Secondary organic aerosol formed by condensing anthropogenic vapours over China's megacities, Nature Geoscience, 10.1038/s41561-022-00922-5, 2022.

Wang, D. S. and Hildebrandt Ruiz, L.: Chlorine-initiated oxidation of n-alkanes under high-NOx conditions: insights into secondary organic aerosol composition and volatility using a FIGAERO–CIMS, Atmos. Chem. Phys., 18, 15535-15553, 10.5194/acp-18-15535-2018, 2018.

Wang, M., Chen, D., Xiao, M., Ye, Q., Stolzenburg, D., Hofbauer, V., Ye, P., Vogel, A. L., Mauldin, R. L., Amorim, A., Baccarini, A., Baumgartner, B., Brilke, S., Dada, L., Dias, A., Duplissy, J., Finkenzeller, H., Garmash, O., He, X.-C., Hoyle, C. R., Kim, C., Kvashnin, A., Lehtipalo, K., Fischer, L., Molteni, U., Petäjä, T., Pospisilova, V., Quéléver, L. L. J., Rissanen, M., Simon, M., Tauber, C., Tomé, A., Wagner, A. C., Weitz, L., Volkamer, R., Winkler, P. M., Kirkby, J., Worsnop,

D. R., Kulmala, M., Baltensperger, U., Dommen, J., El-Haddad, I., and Donahue, N. M.: Photo-oxidation of Aromatic Hydrocarbons Produces Low-Volatility Organic Compounds, Environmental Science & Technology, 54, 7911-7921, 10.1021/acs.est.0c02100, 2020.

Wang, Y., Zhang, Y., Hao, J., and Luo, M.: Seasonal and spatial variability of surface ozone over China: contributions from background and domestic pollution, Atmos. Chem. Phys., 11, 3511-3525, 10.5194/acp-11-3511-2011, 2011.

Wang, Y., Hu, M., Wang, Y., Zheng, J., Shang, D., Yang, Y., Liu, Y., Li, X., Tang, R., Zhu, W., Du, Z., Wu, Y., Guo, S., Wu, Z., Lou, S., Hallquist, M., and Yu, J. Z.: The formation of nitro-aromatic compounds under high NOx and anthropogenic VOC conditions in urban Beijing, China, Atmos. Chem. Phys., 19, 7649-7665, 10.5194/acp-19-7649-2019, 2019.

Wang, Y., Clusius, P., Yan, C., Dällenbach, K., Yin, R., Wang, M., He, X.-C., Chu, B., Lu, Y., Dada, L., Kangasluoma, J., Rantala, P., Deng, C., Lin, Z., Wang, W., Yao, L., Fan, X., Du, W., Cai, J., Heikkinen, L., Tham, Y. J., Zha, Q., Ling, Z., Junninen, H., Petäjä, T., Ge, M., Wang, Y., He, H., Worsnop, D. R., Kerminen, V.-M., Bianchi, F., Wang, L., Jiang, J., Liu, Y., Boy, M., Ehn, M., Donahue, N. M., and Kulmala, M.: Molecular Composition of Oxygenated Organic Molecules and Their Contributions to Organic Aerosol in Beijing, Environmental Science & Technology, 56, 770-778, 10.1021/acs.est.1c05191, 2022.